



Rebecca A. W. Elson; Carl J. Grillmair; Forbes, Duncan A.; Mike Rabban; Gerard. M. Williger; Jean P. Brodie. (1998). HST Imaging of the Globular Clusters in the Fornax Cluster: NGC 1379. *Monthly notices of the Royal Astronomical Society*. 295, (1): 240-250.
Available at: <http://dx.doi.org/10.1046/j.1365-8711.1998.29511307.x>

© 1998 The Royal Astronomical Society.

This is the author's version of the work. It is posted here with the permission of the publisher for your personal use. No further distribution is permitted. If your library has a subscription to this journal, you may also be able to access the published version via the library catalogue.

The definitive version is available at www.interscience.wiley.com

HST Imaging of the Globular Clusters in the Fornax Cluster: NGC 1379

Rebecca A. W. Elson

Institute of Astronomy, Madingley Road, Cambridge CB3 0HA, UK

Electronic mail: elson@ast.cam.ac.uk

Carl J. Grillmair

Jet Propulsion Laboratory, 4800 Oak Grove Drive, Pasadena, CA 91109 USA

Electronic mail: carl@grandpa.jpl.nasa.gov

Duncan A. Forbes

School of Physics and Astronomy, University of Birmingham, Edgbaston, Birmingham B15 2TT, UK

Electronic mail: forbes@star.sr.bham.ac.uk

Mike Rabban

Lick Observatory, University of California, Santa Cruz, CA 95064 USA

Electronic mail: mrabban@ucolick.org

Gerard. M. Williger

Goddard Space Flight Center, Greenbelt, MD 20771 USA

Electronic mail: williger@tejut.gsfc.nasa.gov

Jean P. Brodie

Lick Observatory, University of California, Santa Cruz, CA 95064 USA

Electronic mail: brodie@ucolick.org

Received _____; accepted _____

ABSTRACT

We present B and I photometry for ~ 300 globular cluster candidates in NGC 1379, an E0 galaxy in the Fornax Cluster. Our data are from both Hubble Space Telescope (HST) and ground-based observations. The HST photometry (B only) is essentially complete and free of foreground/background contamination to ~ 2 mag fainter than the peak of the globular cluster luminosity function. Fitting a Gaussian to the luminosity function we find $\langle B \rangle = 24.95 \pm 0.30$ and $\sigma_B = 1.55 \pm 0.21$. We estimate the total number of globular clusters to be 436 ± 30 . To a radius of 70 arcsec we derive a moderate specific frequency, $S_N = 3.5 \pm 0.4$. At radii $r \sim 3 - 6$ kpc the surface density profile of the globular cluster system is indistinguishable from that of the underlying galaxy light. At $r \lesssim 2.5$ kpc the profile of the globular cluster system flattens, and at $r \lesssim 1$ kpc, the number density appears to decrease. The $(B - I)$ colour distribution of the globular clusters (from ground-based data) is similar to that for Milky Way globulars, once corrected for background contamination. It shows no evidence for bimodality or for the presence of a population with $[\text{Fe}/\text{H}] \gtrsim -0.5$. Unlike in the case of larger, centrally located cluster ellipticals, neither mergers nor a multiphase collapse are required to explain the formation of the NGC 1379 globular cluster system.

We stress the importance of corrections for background contamination in ground-based samples of this kind: the area covered by a globular cluster system (with radius ~ 30 kpc) at the distance of the Virgo or Fornax cluster contains $\gtrsim 200$ background galaxies unresolved from the ground, with magnitudes comparable to brighter globular clusters at that distance. The colour distribution of these galaxies is strongly peaked slightly bluer than the peak of a typical globular cluster distribution. Such contamination can thus create the impression of skewed colour distributions, or even of bimodality, where none exists.

Key words: galaxies: individual: NGC 1379 - globular clusters: general - galaxies: star clusters

1. Introduction

An accumulating body of observations suggests that the distribution of colours of globular clusters, and by inference of their metallicities, varies significantly from one galaxy to the next. Of particular interest is the colour bimodality which has now been observed in the globular cluster systems of several large elliptical galaxies, and suggests the presence of distinct metal rich and metal poor populations. The best example is the Virgo cD galaxy M87 (NGC 4486) (cf. Elson & Santiago 1996). It has one population of globular clusters with colours similar to those of the Milky Way globulars, and one which is significantly redder, with inferred metallicities \gtrsim solar. Other galaxies whose globular cluster systems show clear bimodality include M49 (NGC 4472), an E2 galaxy in the Virgo Cluster with the same luminosity as M87 (Geisler, Lee & Kim 1996), and NGC 5846, a slightly less luminous E0 galaxy at the centre of a small compact group (Forbes, Brodie & Huchra 1997a).

Two ideas have been invoked to explain the colour bimodalities. One is that elliptical galaxies are formed during mergers in which populations of metal rich (red) globulars are created and added to a ‘native’ population of metal poor (blue) clusters (cf. Ashman & Zepf 1992). The other is that globular cluster populations with different mean metallicities form during a multiphase collapse of a single system (Forbes, Brodie & Grillmair 1997b): metal poor globular clusters are formed early in the collapse, while metal rich ones form later, roughly contemporaneously with the stars.

To understand fully the implications of the observed colour distributions for the origin of globular cluster systems, a much larger body of accurate data for systems surrounding galaxies of a variety of types and in a variety of environments is required. A question of particular importance, for example, is whether all elliptical galaxies have bimodal globular cluster systems, or whether such systems are restricted to large galaxies in rich environments. The data best suited to address this question are those acquired with the Hubble Space Telescope (HST). The resolution of HST allows even the crowded central regions of galaxies at the distance of Fornax and Virgo to be probed and allows most background galaxies to be eliminated. At these distances samples of globular clusters are complete and uncontaminated to well past the peak of the luminosity function. This paper and the others in this series are contributions to this growing database. Forbes *et al.* (1997a) and Grillmair *et al.* (1997) discuss the globular cluster systems of the Fornax cD galaxy NGC 1399, its neighbour the E1 galaxy NGC 1404, and the peculiar galaxy NGC 1316 which may have undergone a recent merger. Here we present observations of the globular cluster system of NGC 1379, a normal E0 galaxy in the Fornax cluster.

Hanes & Harris (1986) used photographic data to study the NGC 1379 globular cluster system to $B = 23.6$ (about a magnitude brighter than the peak of the luminosity function). They measured the profile of the outer part of the system ($5 < r < 35$ kpc), and estimated the total population to number ~ 800 . More recently the globular cluster systems of five galaxies in the Fornax cluster, including NGC 1379, have been studied by Kohle *et al.* (1996) and Kissler-Patig *et al.* (1997a) using V and I -band photometry obtained with the 100-inch telescope at Las Campanas. Their data are 50% complete at $B \sim 24$, and cover a radial range $\sim 3 - 10$ kpc.

Our observations, obtained both from the ground at the Cerro Tololo Interamerican Observatory (CTIO), and from space using HST, are described in Section 2. Section 3 presents the results, including a caveat concerning the need for accurate background corrections for ground-based data. Our findings are summarized in Section 4.

2. Observations and Data Reduction

In this section we describe the HST and CTIO images upon which our results are based, and the process for detecting, selecting, and determining magnitudes for the globular cluster candidates in each case. We also discuss completeness, and contamination from foreground stars and background galaxies. At an adopted distance of 18.4 Mpc ($m - M = 31.32$; Madore *et al.* 1996), 1 arcsec corresponds to 89 pc. Reddening in the direction of the Fornax cluster is assumed to be negligible (Bender, Burstein, & Faber 1992).

2.1. HST Imaging

Five images of NGC 1379 were obtained with HST on 1996 March 11, using the F450W ($\sim B$) filter. (Due to technical difficulties, the complementary I -band images were not acquired, and are anticipated in 1997.) Three images were taken at one pointing, and two more were offset by 0.5 arcsec. The total exposure time was 5000 seconds. The centre of NGC 1379 was positioned at the centre of the Planetary Camera (PC) chip to afford the greatest resolution in the most crowded regions. Details of the reductions are given by Grillmair *et al.* (1997). Briefly, the images were reduced using the standard pipeline procedure. The

VISTA routine SNUC was used to fit and subtract the underlying galaxy. We ran DAOPHOT II/ALLSTAR (Stetson 1987) separately on the sum of the first three images and the last two images, requiring that detections appear in both lists to qualify as real objects. We adopted a detection threshold of 3σ and measured magnitudes by fitting a point-spread function (PSF). Extended objects were eliminated by visual inspection. Count rates were converted to B magnitudes using the gain ratios and zeropoints given by Holtzman *et al.* (1995; 1997, private communication). Photometry is available on request from CJG.

Figure 1 shows a mosaic of the four WFPC2 chips, with the galaxy subtracted. The total area of the field, excluding two 60 pixel wide unexposed borders on each chip, is 4.8 arcmin^2 . The scale of the Wide Field Camera (WFC) is $0.0996 \text{ arcsec pixel}^{-1}$, and of the PC, $0.0455 \text{ arcsec pixel}^{-1}$. At the distance of NGC 1379, one WFC pixel corresponds to $\sim 9 \text{ pc}$ and one PC pixel to $\sim 4 \text{ pc}$. A globular cluster with size typical of those in the Milky Way (core radius $\sim 2 \text{ pc}$, half-mass radius $\sim 10 \text{ pc}$, and tidal radius $\sim 50 \text{ pc}$) will thus appear essentially unresolved in our images.

A total of ~ 300 objects were detected and measured in our field. To determine the completeness of this sample, 3000 artificial PSFs (100 at each of 30 magnitude levels) were added to the images, and the images were then processed in a manner identical to that for the original data. The completeness of the sample as a function of magnitude is shown in Figure 2. The sample is $\sim 100\%$ complete to $B = 26$ for the WFC chips (80% of the sample), and to $B = 25.5$ for the PC chip. At $B > 26$ the completeness begins to drop rapidly. Photometric errors are $\delta B \approx 0.10 \text{ mag}$ at $B \lesssim 25$, rising to 0.15 mag at $B = 26$.

Next we consider the extent to which our sample may be contaminated by foreground stars and background galaxies. Few foreground stars are expected in an area of only 4.8 arcmin^2 at this Galactic latitude, and most background galaxies are resolved and thus easily distinguished from globular clusters. The main source of contamination is compact, spherical background galaxies. To determine the expected level of contamination in our sample, we observed a background field located ~ 1.4 degrees south of the center of the Fornax cluster. The exposure time was 5200 seconds, so the limit of detection is comparable to that for the NGC 1379 sample. The image was processed and the sample selected in the same way as for the NGC 1379 field (see Grillmair *et al.* 1997).

Figure 3 shows a colour-magnitude diagram (CMD) for the 84 unresolved objects detected in the background field. The sample becomes incomplete at $B > 26.5$, but as we shall see, this is ~ 1.5 magnitudes fainter than the peak of the luminosity function, and so will not affect our results. At $B \lesssim 26.5$ the objects have a wide range of colours, with the majority concentrated around $(B - I) \sim 1$. The B luminosity

function for the background sample is plotted in Fig. 4, which also shows the luminosity function for the ~ 300 candidate globular clusters. The background luminosity function is tabulated in Table 1. Since these background number counts are applicable to HST studies of any unresolved population at high latitude, we also include in Table 1 the I -band luminosity function for the background field. This is plotted as the solid histogram in Fig. 5. As a check on the consistency of the sample, and to assess the amplitude of spatial fluctuations in the background on this scale, we compared the luminosity function in Fig. 5 with the Medium Deep Survey (MDS) star count data from 17 high latitude fields obtained with HST in the V and I bands (Santiago, Gilmore & Elson 1996). The dotted histogram in Fig. 5 shows the I -band luminosity function for the MDS data, normalized to an area of 4.8 arcmin^2 . The two distributions are in excellent agreement to $I \approx 23.5$ which is the limiting magnitude of the MDS star count data. Fainter than this stars can no longer be reliably distinguished from compact galaxies. The MDS stellar luminosity function in V , normalized to the same area, is also included in Table 1. Finally, Fig. 5 also shows a luminosity function for stars and galaxies from the Canada-France Redshift Survey (CFRS) (Lilly *et al.* 1995; S. Lilly 1997, private communication). The magnitudes were measured in an aperture of diameter 3 arcsec. The I -band data cover an effective area of $\sim 425 \text{ arcmin}^2$, and have again been normalized to an area of 4.8 arcmin^2 . These data illustrate the much larger degree of background contamination to be expected in the extreme case where no galaxies (with $I \gtrsim 21$) can be distinguished morphologically from unresolved objects. Background contamination in typical ground-based samples of globular clusters in distant galaxies will fall somewhere between the CFRS and the HST histograms.

2.2. Ground-based Imaging

Broadband B and I images of NGC 1379 were taken with the CTIO 1.5m telescope, using a Tek 2048 x 2048 array with a pixel scale of $0.44 \text{ arcsec pixel}^{-1}$. Total exposure times were 9000 and 3900 seconds for the B and I images respectively. Although the seeing was only $\sim 1.5 \text{ arcsec}$, conditions remained photometric throughout the night of 1995 December 24. Reduction was carried out in the standard way (i.e. bias and dark subtraction, flat-fielding and sky subtraction). After combining, the images were calibrated using aperture photometry from the catalogs of Longo & de Vaucouleurs (1983) and de Vaucouleurs & Longo (1988). This procedure gave an rms precision of better than 0.05 mag.

For the selection of globular cluster candidates in the CTIO images, we employed an iterative procedure using DAOPHOT II. We measured the background noise in both images and set the threshold for single

pixel detection at 5σ , i.e. five times the noise due to the background. The other important detection parameters, SHARPness and ROUNDness (designed to weed out extended objects and cosmic rays), were initially given a large range. For each detected object we measured a 3 pixel radius aperture magnitude and applied an aperture correction based on a curve-of-growth analysis for a dozen isolated globular clusters. The rms error in the aperture correction is ~ 0.05 mag.

We then compared our B -band candidate list with the positions and B magnitudes of globular clusters detected with HST’s WFC. Our candidate list was matched to the HST list with the condition that the HST globular cluster lie within 3 CTIO pixels of our object. With this condition, 28 objects were matched. The average magnitude difference between the CTIO and HST B magnitude is 0.03 mag. Such excellent agreement is gratifying from a photometric standpoint, and reassures us that we have matched the data sets correctly. The matched clusters have SHARPness parameters 0.3 to 0.7 and ROUNDness -0.4 to 0.4 . Assuming that these globular clusters are representative of all globular clusters in the CTIO image, we re-ran DAOPHOT II with the new restricted range in SHARPness and ROUNDness parameters. This resulted in the exclusion of about half the objects in the original sample, which are presumably background galaxies. The same parameters were used for both the B and I images. Figure 6 shows a CMD for 365 objects selected in this way.

A comparison of the CTIO object list and the HST list, within the area in common, will also indicate how complete our detection is as a function of magnitude. The completeness function estimated this way is shown in Fig. 7. Our sample is $\sim 100\%$ complete at $B \sim 21$ and $\sim 50\%$ complete at $B \sim 23.5$. The photometric errors are < 0.1 mag for all magnitudes brighter than our 50% completeness limit.

At this point it is necessary to investigate the level of contamination of our ground-based sample by foreground stars and background galaxies. Since the field is much larger than that observed with HST (211 arcmin^2 compared to 4.8 arcmin^2), and since the resolution is not sufficient to distinguish many background galaxies from unresolved sources, contamination from both stars and galaxies will be significant. Since no background comparison field was obtained, we rely instead on the CFRS data in the B and I -bands, discussed above, to estimate a correction for contamination.

Figure 8 shows histograms of $(B - I)$ for the full NGC 1379 sample in Fig. 6, and for the CFRS sample of objects with $19 < B < 23$. Since selection effects in the two samples are different, we do not normalize the CFRS sample directly using the known area of the survey. Rather, we normalize it to match the tail of objects with $(B - I) > 2.5$ in Fig. 8, whose colours are too red to be globular clusters. From this we

can infer the relative number of contaminants with $(B - I) < 2.5$. The CFRS sample is strongly peaked at $(B - I) \sim 1.0$, which is just ~ 0.4 mag bluer than the peak of the NGC 1379 sample. The NGC 1379 sample is lacking many of the bluest objects in the CFRS sample; this is probably because fainter galaxies are on average bluer, and the CFRS sample is much more complete than the NGC 1379 sample at the faintest magnitudes. Also, our process of excluding galaxies from the CTIO sample on the basis of ROUNDness would preferentially eliminate edge-on spirals, which are systematically bluer than ellipticals. The most important point illustrated by Fig. 8 is that in the ground-based data, much more so than in the HST data, failure to properly correct for foreground/background contamination may lead to a significant error in the deduced colour of the peak of the globular cluster colour distribution, and possibly to the erroneous impression of a bimodal colour distribution. With ground-based data obtained with better seeing it would of course be possible to exclude a greater proportion of background galaxies, so that any skewing of the colour distribution would be less severe.

3. Properties of the NGC 1379 globular cluster system

The principal properties of a globular cluster system which any theory of its origin and evolution must account for are the luminosity function (in particular, the absolute magnitude of its peak, and the width of the distribution), the colour distribution (in particular, the colour of the peak and the presence or absence of any bimodality), the radial distribution, and the total number of clusters, N_{tot} , and therefore the specific frequency, defined as $S_N = N_{tot} 10^{0.4(M_V + 15)}$, where M_V is the absolute magnitude of the galaxy. With $B_{tot} = 12.07$ (Tully 1988) and $(B - V) = 0.89$ (Faber *et al.* 1989) we infer an apparent magnitude for NGC 1379 of $V_{tot} = 11.18$. With distance modulus 31.32, this implies $M_V = -20.16$. This is the integrated magnitude within a radius of ~ 70 arcsec.

3.1. Luminosity function

The luminosity function for the NGC 1379 globular cluster candidates derived from the HST data is shown in Fig. 4. This sample includes ~ 300 unresolved objects and is essentially complete and uncontaminated well past the peak. The background-corrected luminosity function, that is, the difference

between the solid and dashed histograms in Fig. 4, is shown in Fig. 9. Fitting a Gaussian function to the luminosity function in Fig. 4, using a maximum-likelihood technique which is independent of binning, and takes into account completeness, background contamination, and photometric errors (Secker & Harris 1993), we derive a peak magnitude of $\langle B \rangle = 24.95 \pm 0.30$, and a width $\sigma_B = 1.55 \pm 0.21$. This Gaussian is shown as the solid curve in Fig. 9.

We know of no other direct measurements of $\langle B \rangle$ for this system to compare with ours. However, our values are the same, to within the errors, as the values measured for the globular cluster systems of two other Fornax galaxies, NGC 1399 and NGC 1404 (Grillmair *et al.* 1997). Also, for four elliptical galaxies in the Virgo cluster Harris *et al.* (1991) find an average value $\langle B \rangle = 24.77 \pm 0.2$. Combining this with the value $(m - M)_{Fornax} - (m - M)_{Virgo} = 0.08 \pm 0.09$ (Kohle *et al.* 1996) implies $\langle B \rangle = 24.85 \pm 0.22$ for NGC 1379. This is in good agreement with our value.

We may either use the measured peak magnitude to infer a distance modulus for NGC 1379, assuming a ‘universal’ value for the absolute magnitude of the peak, or we may adopt a distance modulus and infer an absolute magnitude. While the value of $\langle M_V \rangle$ has been measured for many globular cluster systems, there are fewer B -band studies. Sandage & Tamman (1995) quote $\langle M_B \rangle = -6.93 \pm 0.08$ for the Milky Way and M31 globular clusters, while Ashman, Conti & Zepf (1995) give $\langle M_B \rangle = -6.50$ for the Milky Way clusters. Adopting the Cepheid distance for NGC 1379 and our measured peak magnitude, implies $\langle M_B \rangle = -6.37 \pm 0.36$, which is in good agreement with the Ashman *et al.* value and somewhat fainter than the Sandage & Tamman value.

As we shall see below, the $(B - I)$ distribution of NGC 1379 globular clusters appears very similar to that for the Milky Way globular clusters. It should therefore be safe to assume that the $(B - V)$ distribution is also similar. Adopting $\langle B - V \rangle = 0.7$ for the Milky Way globulars (Harris 1996), we may convert our value for the peak magnitude of the luminosity function, $\langle B \rangle = 24.95 \pm 0.30$, to $\langle V \rangle = 24.25 \pm 0.30$. This value is somewhat fainter than the value found by Kohle *et al.* (1996) of $\langle V \rangle = 23.68 \pm 0.28$, but their data reach just to the peak of the luminosity function, and the errors in their faintest bin are large. The sense of the difference is consistent with our result above that fitting only the brighter part of the luminosity function results in a peak magnitude which is too bright. With the Cepheid distance modulus of 31.32, our $\langle V \rangle$ value implies $\langle M_V \rangle = -7.07 \pm 0.36$, which is typical for elliptical galaxies of this absolute magnitude (Harris 1991).

Our value of $\sigma_B = 1.55 \pm 0.21$ for the NGC 1379 globular cluster system is larger than the values

$\sigma_B = 1.07$ and 0.89 quoted by Sandage & Tamman for the Milky Way and M31 respectively, but is consistent with the values $\sigma_B = 1.37 \pm 0.07$ and $\sigma_B = 1.39 \pm 0.12$ found by Grillmair *et al.* (1997) for the globular cluster systems of NGC 1399 and NGC 1404 respectively. It is also consistent with the value $\sigma_B = 1.46 \pm 0.07$ for four elliptical galaxies in the Virgo cluster (Harris *et al.* 1991).

3.2. Radial profile

Harris & Hanes (1987) compared the radial profile of the NGC 1379 globular cluster system with the surface brightness profile of the galaxy itself from Schombert (1986), over the radial range $5 - 35$ kpc. They detected no difference between the two, although their uncertainties were large. Kissler-Patig *et al.* (1997a) found the same result from their ground-based data over the range $3 - 10$ kpc. Radial surface density profiles for our HST sample of NGC 1379 globulars are shown in Figs. 10a and b. Corrections have been made to compensate for the fraction of each annulus which falls outside the field of view of the WFPC2. In Figure 10a profiles are plotted for both the complete, uncontaminated sample with $B < 25.5$, and for the objects with $B > 26.5$ (with no correction for completeness), which are expected to be primarily background galaxies. Indeed, the fainter sample shows almost no radial gradient. The dashed line is the background level (~ 9.0 objects per arcmin²) measured from the background field for $B > 26.5$. The agreement is excellent. The background level for the brighter sample, again measured from the background field, is 2.7 objects per arcmin², and is shown as the solid line. The difference between the radial profile and the background level is probably due to small numbers, but may indicate a small amount of residual contamination: the five outermost points represent an average of < 4 objects each, and the total number of objects in the background field with $B < 25.5$ is just 13.

The radial profile of the brighter sample decreases smoothly from $\sim 10 - 80$ arcsec ($\sim 1 - 7$ kpc), at which point the globular cluster system is lost in the background. Figure 10b shows the radial profile for the sample with $B < 25.5$, with a background of 2.7 objects per arcmin² subtracted. Superposed is a curve representing the surface brightness profile of the underlying galaxy from Kissler-Patig *et al.* (1997a), scaled arbitrarily to match the profile of the globular cluster system. The two profiles agree well at $\sim 35 - 70$ arcsec ($3-6$ kpc). There is no evidence that the surface brightness profile of the globular cluster system is shallower than that of the underlying galaxy light out at least to the limit of our data at $r \sim 7$ kpc. The logarithmic slope of the profile in Fig. 10b is -2.4 at $r \gtrsim 35$ arcsec.

Inwards of $r \sim 30$ arcsec (~ 2.5 kpc) the profile of the globular cluster system flattens out. This core structure seems to be a common feature of the globular cluster systems of elliptical galaxies, and the radius at which the flattening occurs correlates with the galaxy luminosity (Forbes *et al.* 1996). The mean surface density within ~ 10 arcsec of the centre of NGC 1379 is $\sim 200 \pm 60$ clusters per arcmin². The core radius, where the surface density has fallen to half its central value, is $r_c \sim 23 \pm 6$ arcsec (2.0 ± 0.5 kpc). This is consistent with values for other galaxies with absolute magnitude comparable to that of NGC 1379. Such a core structure is not present in the underlying galaxy light, which, while it changes slope slightly at $r \sim 50$ arcsec, rises with constant slope inwards to at least 10 arcsec (Schombert 1986).

Inwards of ~ 10 arcsec (~ 1 kpc), the surface density of globular clusters appears to decrease. This radius corresponds to 220 pixels on the PC, and as can be seen from Fig. 1, crowding even in these inner regions is not severe. Extrapolating a smoothly rising profile to the center of the galaxy would require 6 clusters instead of 2 in the innermost bin, and 14 instead of 12 in the second bin. If the radial distribution really were steadily rising, this would imply that our data are only $\sim 70\%$ complete in these combined bins. Closer analysis of our completeness tests reveals that we are in fact 97% complete for $B < 25.5$ in the region $r < 220$ pixels (the slight reduction over the PC-averaged completeness value being a consequence of the increased noise due to the integrated stellar light of the central regions of the galaxy). We conclude that the central dip in the cluster surface density distribution is not an artifact of our analysis, and may indeed indicate a quite substantial drop in the volume density of clusters near the nucleus of the galaxy. Radii less than 1 kpc from the nucleus are where we expect tidal stresses to begin to take a toll on the numbers of globular clusters (Lauer & Kormendy 1986, Grillmair, Pritchet, & van den Bergh 1986), either during their formation or subsequently through tidal stripping (Grillmair *et al.* 1995), particularly if the clusters are on box orbits.

We now turn to the ground-based data which cover a much greater area than the HST data. The radial distribution for the full sample from Fig. 6 is shown in Fig. 11. The surface density for the CTIO sample has been increased by 0.74 in $\log N$ to match the HST sample, which is shown as the solid curve. At $r \gtrsim 100$ arcsec, the profile of the CTIO sample is essentially flat, suggesting that the sample is composed overwhelmingly of foreground/background objects at these radii. Even a colour selection is unlikely to help disentangle the background contamination since, as shown in Fig. 8, background galaxies have a similar colour distribution to the full NGC 1379 sample. We therefore conclude that, despite the larger spatial coverage of the ground-based sample, in the absence of a suitable background calibration field it does not contribute much to our knowledge of the radial structure of the NGC 1379 globular cluster system not

covered by our HST data. It is also unable to probe the innermost regions of the cluster system, due to crowding.

3.3. Colour distribution

In the absence of an I -band image from HST, we attempt to extract a sample of globular clusters from the ground-based data which is as uncontaminated as possible, to investigate the $(B - I)$ colour distribution. One approach is to select only objects with $r < 100$ arcsec, since these show a radial gradient in surface density (Fig. 11). This gives a sub-sample of 35 objects. The background level inferred from the radial distribution of the CTIO sample at $r > 100$ arcsec is 1.6 arcmin^{-2} , implying that 14 of the 35 globular cluster candidates at $r < 100$ arcsec, or 40% of this sample, are background galaxies or foreground stars.

The colour distribution for the 35 objects at $r < 100$ arcsec, along with those for the full CTIO sample and for the CFRS sample, is shown as the dashed histogram in Fig. 8. The $r < 100$ arcsec sample clearly peaks at a redder colour than the full sample, underlining the fact that the colour distribution of the uncorrected sample is misleading. Figure 12 shows the same histogram for the $r < 100$ arcsec sample, along with the histogram of residuals obtained by subtracting the normalized CFRS histogram from the full CTIO histogram in Fig. 8. A histogram for 95 globular clusters in the Milky Way (Harris 1996) is also shown. The colour distributions of the NGC 1379 sample with $r < 100$ arcsec, and with the CFRS sample subtracted, have a very similar peak colour, $(B - I) \approx 1.6$, which is indistinguishable from that for the globular cluster system of the Milky Way.

Using the relation between $(B - I)$ colour and metallicity from (Couture *et al.* 1990) we infer from the peak colour a metallicity of $[\text{Fe}/\text{H}] \sim -1.5$. Forbes *et al.* (1997b) plot a relation between mean metallicity of globular clusters and parent galaxy magnitude for 11 galaxies with $-21 < M_V < 23$, with bimodal globular cluster colour distributions. They find that, while in the metal rich populations ($[\text{Fe}/\text{H}] > -0.5$) there is a strong correlation between mean globular cluster metallicity and galaxy magnitude, for the metal poor populations the scatter is much greater and the correlation much weaker. There is, however, a trend for less luminous galaxies to have globular clusters with a lower mean metallicity, and our results for NGC 1379 are consistent with this trend.

There is a tail of bluer objects in the NGC 1379 samples which is probably comprised of residual

background galaxies. If these objects were globular clusters, their colours would imply metallicities of $[\text{Fe}/\text{H}] \lesssim -2.5$. The objects with $(B - I) \gtrsim 2.5$ are again probably residual stars or galaxies. Even the most metal rich globular clusters in the Milky Way have $(B - I) \lesssim 2.0$, and a metal rich population of clusters, such as appears to exist in M87, would have $(B - I) \sim 2$. We see no evidence for the presence of a population of clusters with $[\text{Fe}/\text{H}] \gtrsim -0.5$ in NGC 1379, nor for a bimodal distribution of metallicities, although confirmation of this result must await the acquisition of the complementary I -band image of our field with HST.

It is interesting to compare the mean colour of the NGC 1379 globular clusters with the colour of the underlying galaxy. Pickles & Visvanathan (1985) present multicolour photometry for a sample of Fornax galaxies including NGC 1379. Their results imply $(B - I) \sim 2.0$ in an aperture of diameter 45 arcsec. This is significantly redder than the mean colour of the clusters, and indicates that, as has been found in other galaxies (cf. Harris 1991), the globular clusters of NGC 1379 are significantly more metal poor than the halo stars.

3.4. Total number and specific frequency

We can estimate the total size of the NGC 1379 globular cluster population from our HST data. Considering only globular clusters in the bright half of the luminosity function (with $B < 24.95$), and making corrections for the area of each annulus that falls outside the WFPC2 field of view (typically $\sim 50 - 60\%$), we estimate that to $r = 100$ arcsec, there are 218 globular clusters. Multiplying by two to include the faint half of the luminosity function, we infer a total number $N_{tot} = 436 \pm 30$. Beyond 100 arcsec the globular cluster system is lost in the background. Since in an annulus at $100 - 200$ arcsec we would expect ~ 50 background objects, the number of globular clusters at these radii that have gone undetected must be a small fraction of 50.

Our estimate of N_{tot} is consistent with the value 380 ± 100 quoted by Harris (1996), and is 40% larger than the value 314 ± 63 estimated by Kissler-Patig *et al.* (1997a). Our HST observations of the inner regions of the globular cluster system have reduced the uncertainty in N_{tot} considerably over estimates from ground-based studies. To $r = 70$ arcsec we estimate $N_{r < 70} = 396 \pm 44$. Adopting $V_{tot} = 11.18$ for NGC 1379 from Tully (1988), which is the integrated magnitude within $r = 70$ arcsec, and the distance modulus 31.32, we derive a specific frequency $S_N = 3.5 \pm 0.4$. This value is typical for E/S0 galaxies of this

magnitude (Harris 1991; Forbes *et al.* 1997b).

4. Summary

The properties of the NGC 1379 globular cluster system derived in our study are summarized in Table 2. In its luminosity function and specific frequency, it appears to be typical of globular cluster systems in elliptical galaxies of this magnitude. The colour distribution of the globular clusters in NGC 1379 is similar to that of the Milky Way globular clusters. In particular, there is no evidence for bimodality or for the presence of a population of clusters with $[\text{Fe}/\text{H}] \gtrsim -0.5$. Structurally, the outer part of the cluster system ($r > 3$ kpc) has the same surface density profile as the underlying galaxy light, as suggested by previous studies (Harris & Hanes 1987; Kissler-Patig *et al.* 1997a).

The similarity of the profiles of the galaxy and globular cluster system is not consistent with the predictions of merger models (cf. Ashman & Zepf 1992), which suggest that globular clusters formed during mergers are dynamically heated, and the resulting system has a profile which is shallower than that of the underlying galaxy. Neither is a multiphase collapse model required to explain these observations, as there is no evidence of a second phase of globular cluster formation from enriched gas. Indeed, NGC 1379 appears to be an example of an elliptical galaxy whose globular clusters formed *in situ* in a single phase collapse, unlike the larger centrally located ellipticals, including M87, NGC 1399, and NGC 5846, which may require either mergers or a multiphase collapse to explain their globular cluster systems. This result supports the suggestion of Kissler-Patig *et al.* (1997b) that low luminosity elliptical galaxies ($M_V \gtrsim -21.5$) have globular cluster systems that formed early in a single collapse, and have remained essentially unperturbed.

Finally, we stress the importance of applying background corrections to data obtained from the ground. At the distance of the Fornax or Virgo cluster, a globular cluster system with radius 30 kpc will cover an area that will contain ~ 200 background galaxies with $B \lesssim 25$, unresolved even with HST. A field with radius 10 kpc will contain ~ 20 such objects. The colour distribution of the background galaxies is strongly peaked at $(B - I) \sim 1.0$. Superposed on a distribution of somewhat redder globular clusters, this can create the impression of a skewed distribution or even of a bimodal one, where none exists. The background galaxies would mimic a metal poor (blue) globular cluster population rather than a metal rich (red) one. On the other hand, an HST WFPC2 field with size ~ 4.8 arcmin² will generally contain negligible numbers of foreground stars and background galaxies to $B \sim 26$. While corrections are desirable in either case, they

are important in the case of ground-based observations of sparser globular cluster systems, the results of which may otherwise be misleading.

Acknowledgments

This research was funded in part by the HST grant GO-05990.01-94A and by Faculty Research funds from UCSC.

References

- Ashman, K. & Zepf, S. 1992 *Astrophys. J.* 384, 50
- Bender, R., Burstein, D., & Faber, S. M. 1992 *Astrophys. J.* 399 462
- Couture, J., Harris, W. & Allwright, J. 1990 *Astrophys. J. Suppl.* 73, 671
- Elson, R. A. W. & Santiago, B. X. 1996 *Mon. Not. R. astr. Soc.* 280, 971
- Faber, S. M., Wegner, G., Burstein, D., Davies, R. L., Dressler, A., Lynden-Bell, D. & Terlevich, R. J. 1989 *Astrophys. J. Suppl.* 69, 763
- Forbes, D. A., Brodie, J. & Huchra, J. 1997a *Astr. J.* 113, 887
- Forbes, D., Franx, M., Illingworth, G. & Carollo, C. 1996 *Astrophys. J.* 467, 126
- Forbes, D. A., Brodie, J. & Grillmair, C. G. 1997b *Astr. J.* in press
- Forbes, D. A., Grillmair, C. G., Williger, G., Elson, R. & Brodie, J., 1997a, *Mon. Not. R. astr. Soc.* in press
- Geisler, D., Lee, M. G. & Kim, E. 1996 *Astr. J.* 111, 1529
- Grillmair, C. J., Forbes, D. A., Brodie, J. & Elson, R. A. W. 1997, *Astr. J.* submitted
- Grillmair, C. J., Freeman, C. J., Irwin, M., & Quinn, P. J. 1995, *Astr. J.* , 109, 2553
- Grillmair, C. J., Pritchett, C. J., & van den Bergh, S. 1986, *Astr. J.* , 91, 1328
- Hanes, D. A. & Harris, W. E. 1986 *Astrophys. J.* 309, 564
- Harris, W. E. 1991 *Ann. Rev. Astr. Ap.* 29, 543
- Harris, W. E. 1996 *Astr. J.* 112, 1487

- Harris, W. E., Allwright, W. Pritchett, C. & van den Bergh, S. 1991 *Astrophys. J. Suppl.* 76, 115
- Harris, W. E. & Hanes, D. A. 1987 *Astr. J.* 93, 1368
- Holtzman, J. *et al.* 1995 *Pub. Astr. Soc. Pac.* 107, 1065
- Kissler-Patig, M., Kohle, S., Hilker, M., Richtler, T., Infante, L., & Quintana, H. 1997b *Astr. Ap.* 319, 83
- Kissler-Patig, M., Kohle, S., Hilker, M., Richtler, T., Infante, L., & Quintana, H. 1997a *Astr. Ap.* 319, 470
- Kohle, S., Kissler-Patig, M., Hilker, M., Richtler, T., Infante, L., & Quintana, H. 1996 *Astr. Ap.* 309, L39
- Lauer, T. R., & Kormendy, J. 1986, *Astrophys. J.* , 301, L1
- Lilly, S., Le Fevre, O., Crampton, D., Hammer, F. & Tresse, L. 1995 *Astrophys. J.* 455, 50
- Longo, G., & de Vaucouleurs, A. 1983, *A General Catalogue of Photometric Magnitudes and Colors in the UB system* (University of Texas, Austin)
- Madore, B. *et al.* 1996, *Bulletin of the American Astronomical Society* 189, 108.04
- Pickles, A. & Visvanathan, V. 1985 *Astrophys. J.* 294, 134
- Santiago, B. X., Gilmore, G. & Elson, R. A. W. 1996 *Mon. Not. R. astr. Soc.* 281, 871
- Schombert, J. M. 1986 *Astrophys. J. Suppl.* 60, 603
- Secker, J. & Harris, W. 1993 *Astr. J.* 105, 1358
- Stetson, P. B. 1987 *Pub. Astr. Soc. Pac.* 99, 191
- Tully, B. 1988 *Nearby Galaxies Catalog*, Cambridge University Press, Cambridge
- de Vaucouleurs, A. & Longo, G. 1988 *A Catalogue of Visual and Infra-Red Photometry of Galaxies from 0.5 μ m to 10 μ m*, Univ. of Texas, Austin

Figure Captions

Figure 1. F450W($\sim B$) image of the NGC 1379 globular cluster system. The underlying galaxy, centred on the smaller PC chip, has been subtracted. The mosaic is 147 arcsec on a side.

Figure 2. Completeness as a function of B magnitude for the HST sample, for the WFC chips (solid curves) and the PC chip (dashed curve). Our HST sample is $\sim 100\%$ complete to $B \sim 26$ for the WFC chips which contain $\sim 80\%$ of the clusters, and to $B \sim 25.5$ for the PC chip.

Figure 3. Colour-magnitude diagram for 84 unresolved objects detected in a background field 1.4 degrees from the center of the Fornax cluster, observed with HST.

Figure 4. B -band luminosity functions for the HST sample of NGC 1379 globular cluster candidates (solid histogram), and the unresolved objects in the background field (dashed histogram). The vertical dotted line shows the limit of $\sim 100\%$ completeness of the NGC 1379 sample.

Figure 5. I -band luminosity functions for the objects in the Fornax background field (solid histogram), for Galactic stars from the Medium Deep Survey in 17 high latitude fields (dotted histogram), and for galaxies and stars from the CFRS (dashed histogram). All luminosity functions are normalized to 1.0 mag bins and an area of 4.8 arcmin². The original areas are 4.8 arcmin² for the Fornax background field, 82 arcmin² for the MDS starcounts, and ~ 425 arcmin² for the CFRS sample.

Figure 6. Colour-magnitude diagram for 365 objects with $0.3 < \text{SHARPness} < 0.7$ and $-0.4 < \text{ROUNDness} < 0.4$ in the CTIO image of NGC 1379. Representative error bars are shown.

Figure 7. Completeness as a function of B magnitude for the CTIO sample shown in Fig. 6, determined by comparison with the HST sample. The CTIO sample is $\sim 100\%$ complete at $B \sim 21$ and $\sim 50\%$ complete at $B \sim 23.5$.

Figure 8. $(B - I)$ distributions for objects in the CTIO sample (solid histogram), and in the CFRS sample (dotted histogram) for the magnitude range indicated. The CFRS sample has been normalized to match the CTIO histogram at $(B - I) > 2.5$. The dashed histogram is the $(B - I)$ distribution for the CTIO sample of objects with galactocentric distance $r < 100$ arcsec (~ 9 kpc).

Figure 9. B luminosity function from Fig. 4 corrected for contamination by subtracting the background luminosity function shown as the dashed histogram in Fig. 4. The maximum-likelihood best fitting Gaussian function is shown as the solid curve, and has $\langle B \rangle = 24.95 \pm 0.30$ and $\sigma_B = 1.55 \pm 0.21$.

Figure 10. Surface density profiles (number per arcmin²) for objects in the HST sample. (a) The filled circles are for globular cluster candidates with $B < 25.5$, to which limit the sample is expected to be both complete and uncontaminated. The open circles are for objects with $B > 26.5$, which are probably mostly background galaxies. The solid horizontal and dashed lines indicate the background level derived from the HST background field for $B < 25.5$ and for $B > 26.5$ respectively. The cluster system can be traced to a radius of 80 arcsec (~ 7 kpc). The average number of clusters observed in the last 5 bins is < 4 . The dip in the number of clusters in the central ~ 10 arcsec appears to be real. (b) Radial profile for the sample of globular clusters with $B < 25.5$ with a background of 2.7 objects per arcmin² subtracted. The dotted curve is the surface brightness profile of the underlying galaxy, arbitrarily normalized to match the radial profile of the cluster system. Poisson errorbars are shown.

Figure 11. Surface density profiles (number per arcmin²) for the CTIO sample (filled circles), and the HST sample with $B < 25.5$ (solid curve). Poisson errorbars are shown. The CTIO surface density profile has been increased by 0.74 in $\log N$ to match the HST distribution. Beyond ~ 100 arcsec (~ 9 kpc) the CTIO sample shows no radial gradient. The solid horizontal line corresponds to a background density of ~ 9 objects per arcmin².

Figure 12. $(B - I)$ distributions for the CTIO sample of NGC 1379 globular cluster candidates with galactocentric radius < 100 arcsec (shaded histogram), for the background (CFRS) corrected sample (solid histogram), and for 95 globular clusters in the Milky Way (dashed histogram).

Table 1: Luminosity functions for unresolved objects in high Galactic latitude HST fields .

B	N_{bck}	I	N_{bck}	N_{MDS}	V	N_{MDS}
20.25	0	18.25	0	0	19.25	0
20.75	0	18.75	1	0.18	19.75	0.13
21.25	0	19.25	1	0.76	20.25	0.19
21.75	0	19.75	0	1.41	20.75	0.36
22.25	0	20.25	0	1.47	21.25	0.85
22.75	1	20.75	0	1.88	21.75	0.74
23.25	2	21.25	2	1.82	22.25	1.65
23.75	1	21.75	2	2.35	22.75	1.53
24.25	0	22.25	1	2.47	23.25	2.27
24.75	3	22.75	5	2.24	23.75	2.02
25.25	6	23.25	2	3.00	24.25	2.02
25.75	8	23.75	5	1.18	24.75	2.08
26.25	19	24.25	6	0.41	25.25	2.51
26.75	13	24.75	11	0	25.75	1.78
27.25	12	25.25	11			
27.75	13	25.75	16			
28.25	6	26.25	17			
28.75	0	26.75	4			
29.25	0	27.25	0			
29.75	0	27.75	0			

Notes: Magnitudes are in the Johnson-Cousins system. Columns 2 and 4 are numbers of unresolved objects (stars and galaxies) per unit magnitude in our HST background field with area 4.8 arcmin^2 , 1.4 degrees south of the centre of the Fornax cluster. Columns 5 and 7 are star counts from 17 high latitude HST fields observed as part of the Medium Deep Survey. Numbers are per unit magnitude, and are normalized to the area of a single WFPC2 field (4.8 arcmin^2).

Table 2: Properties of the NGC 1379 globular cluster system.

$\langle B \rangle = 24.95 \pm 0.30$	$N_{tot} = 436 \pm 30$	$\langle M_B \rangle = -6.37 \pm 0.36$
$\sigma_B = 1.55 \pm 0.21$	$r_{core} = 2.0 \pm 0.5$ kpc	$\langle M_V \rangle = -7.07 \pm 0.36$
$\langle B - I \rangle \approx 1.6$	$\alpha = -2.4$	$S_N = 3.5 \pm 0.4$
		$[\text{Fe}/\text{H}] \approx -1.5$

Notes: Properties in columns 1 and 2 are derived directly from our data. Properties in column 3 are inferred assuming a distance modulus of 31.32, a colour for globular clusters of $\langle B - V \rangle = 0.7$, a total magnitude for NGC 1379 of $M_V = -20.16$, and a relation between $(B - I)$ and $[\text{Fe}/\text{H}]$ from Couture *et al.* (1990). No correction for Galactic extinction has been applied to any of these quantities, as it is assumed to be negligible. The value of S_N is for $r \lesssim 70$ arcsec.

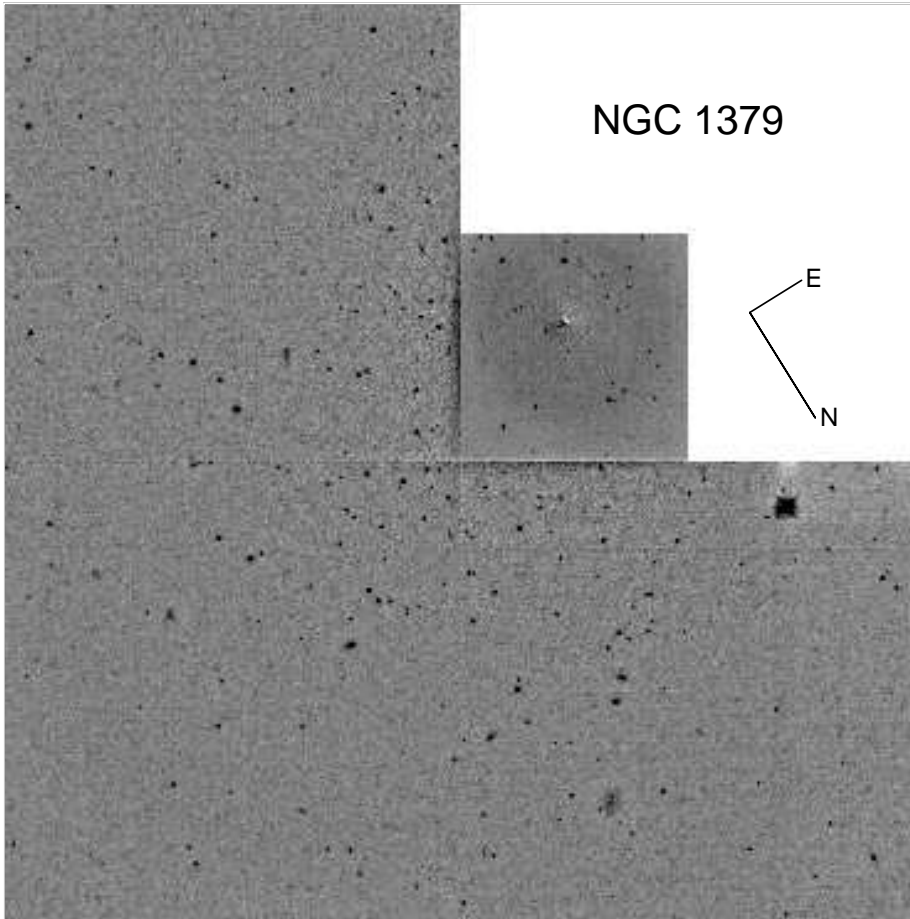


Fig. 1.—

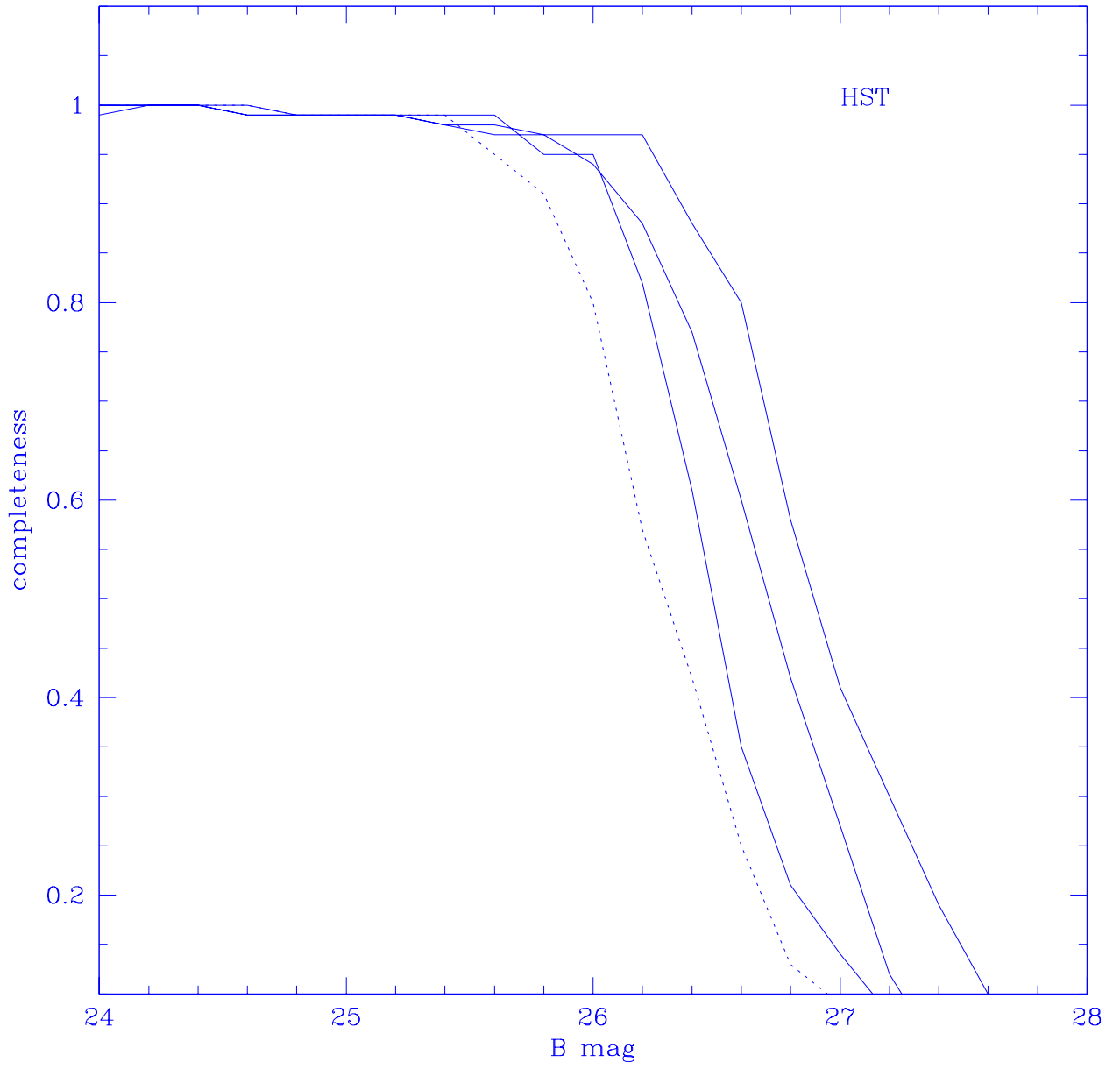


Fig. 2.—

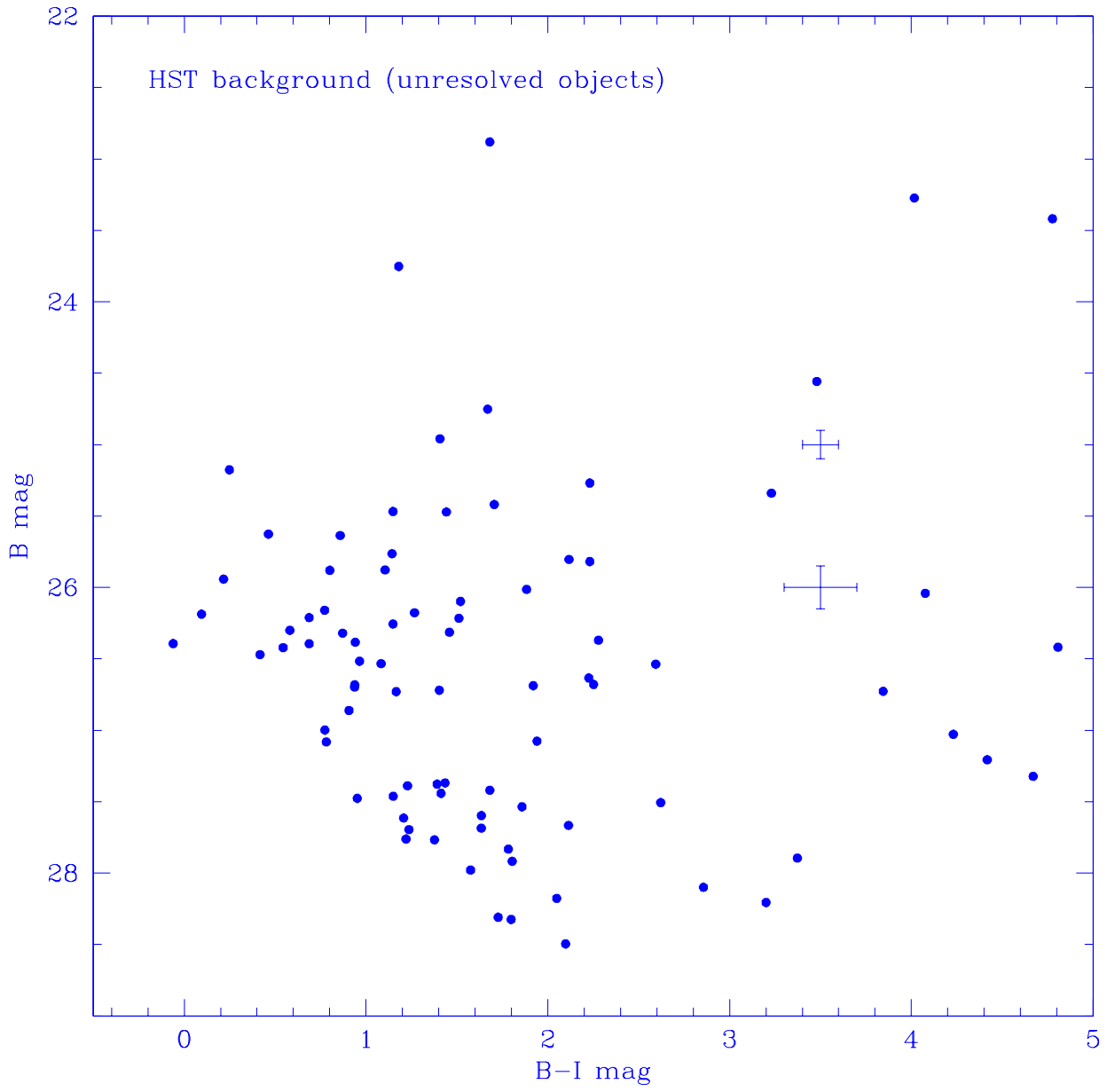


Fig. 3.—

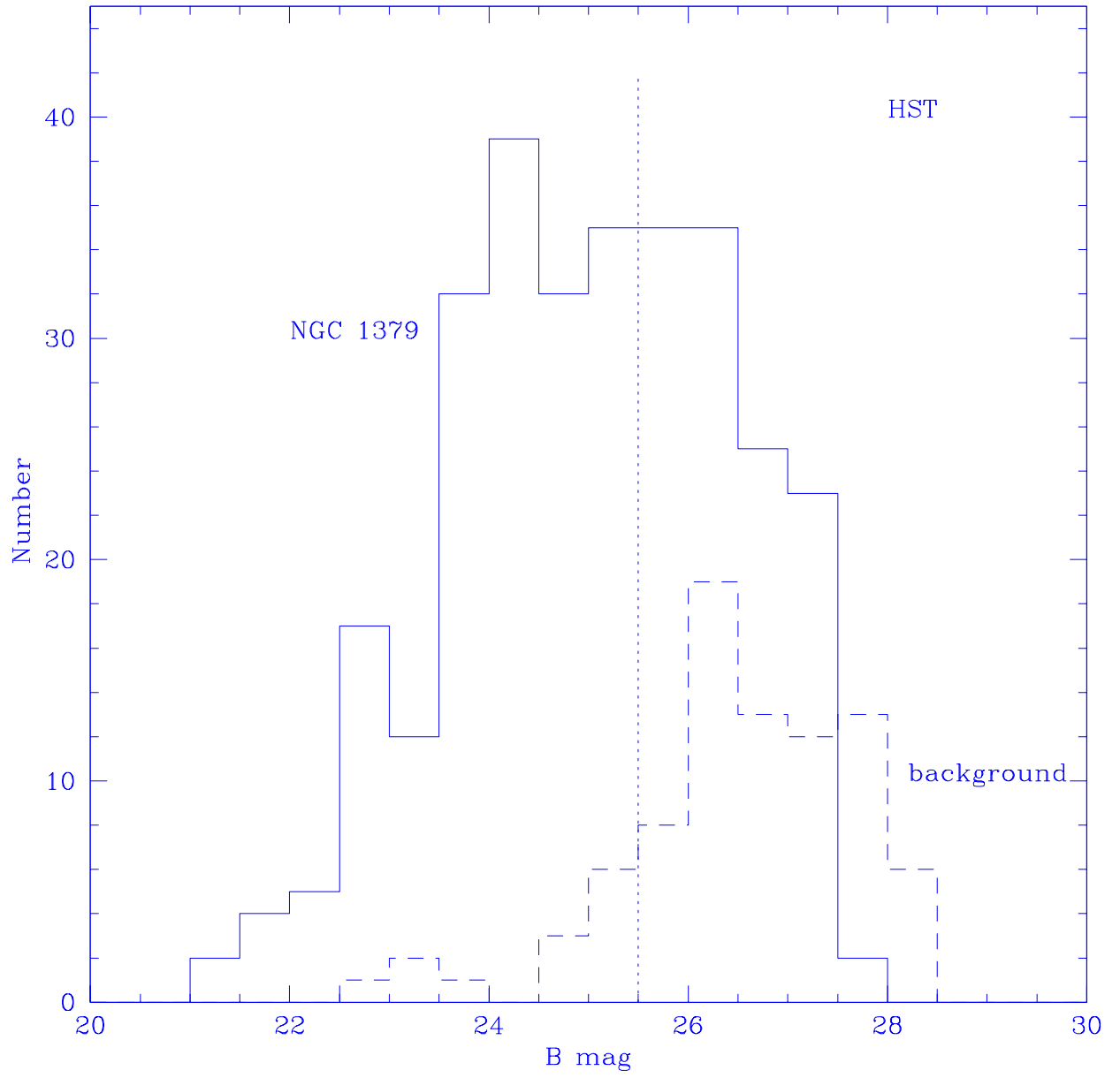


Fig. 4.—

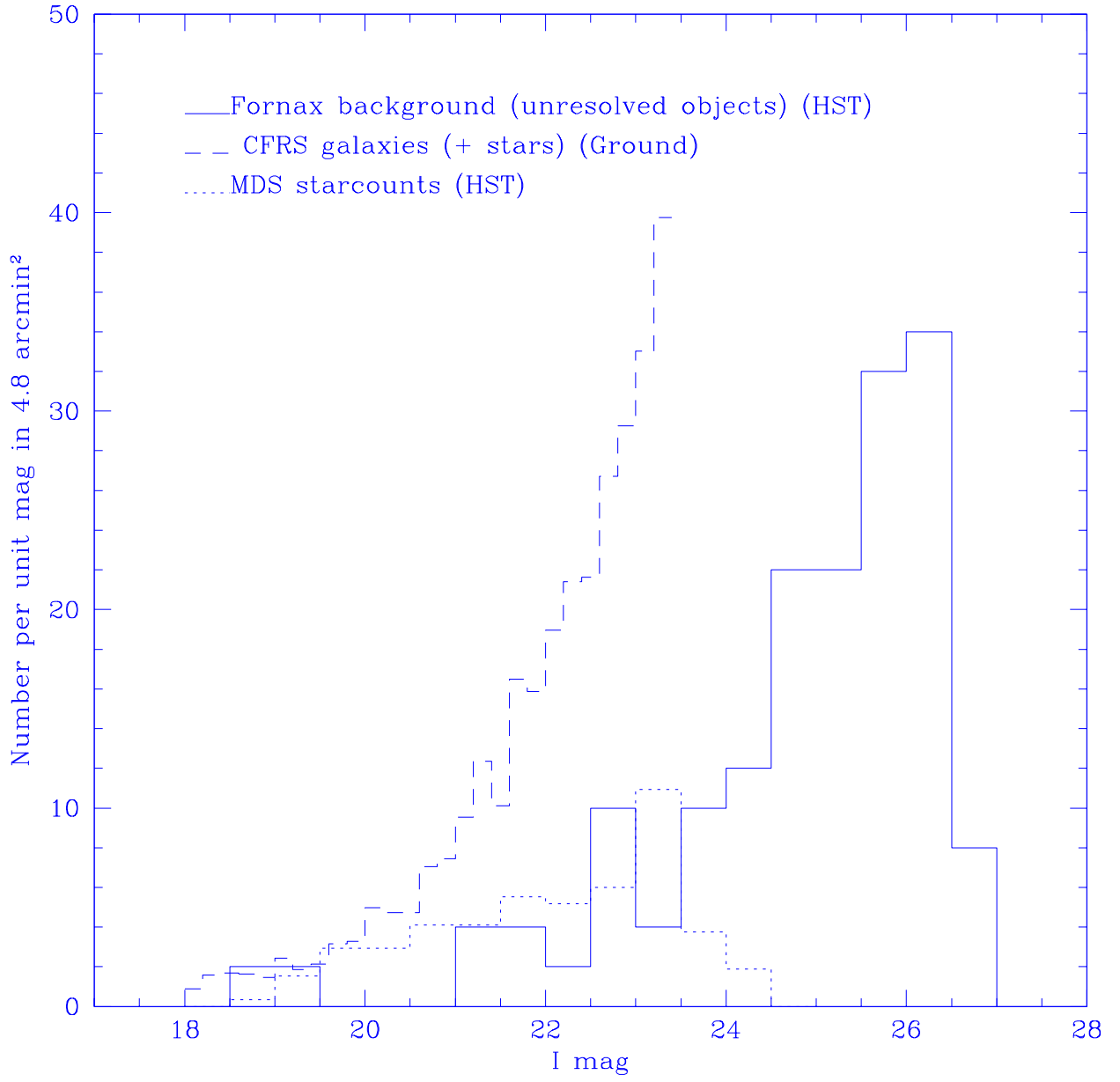


Fig. 5.—

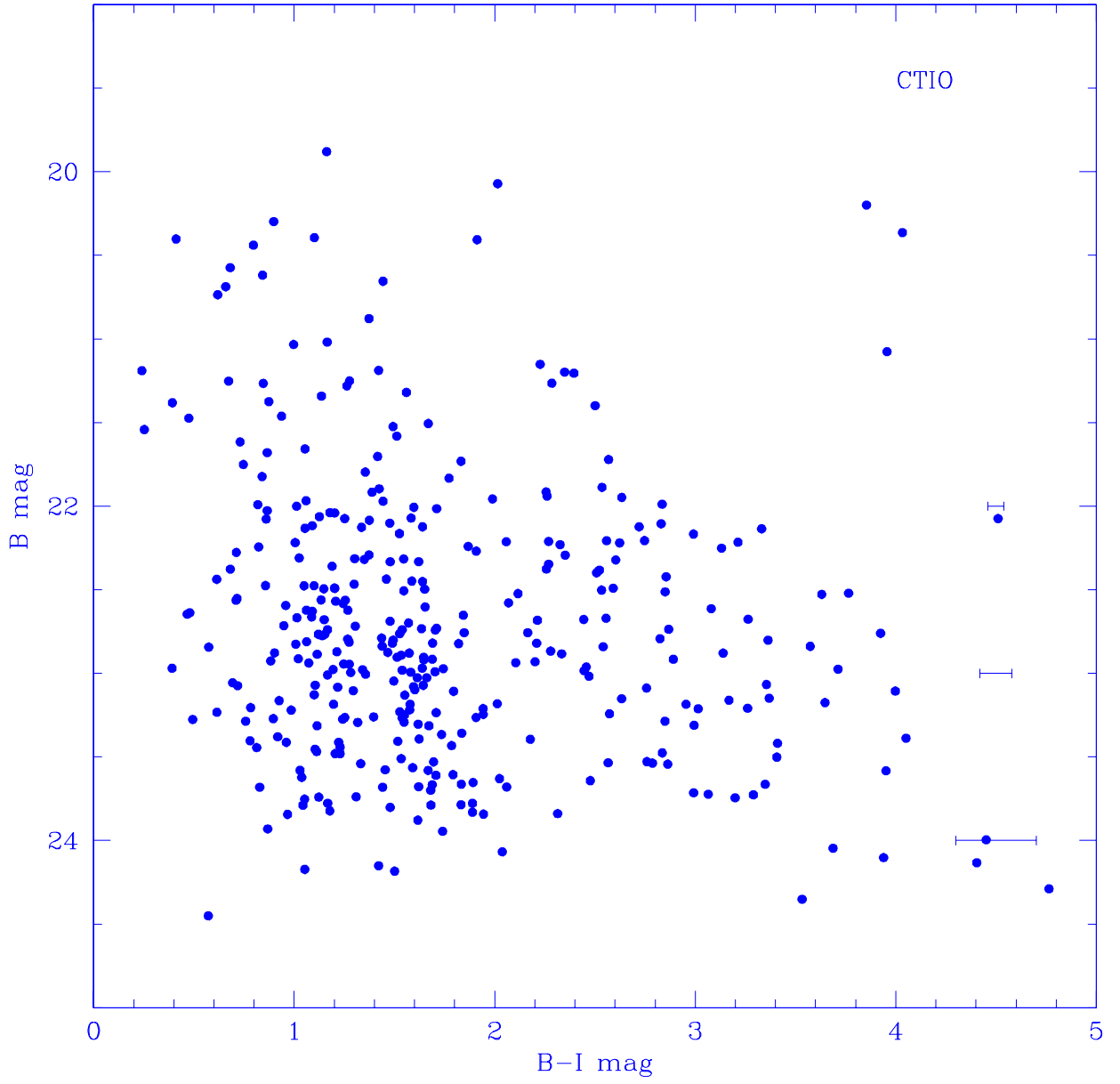


Fig. 6.—

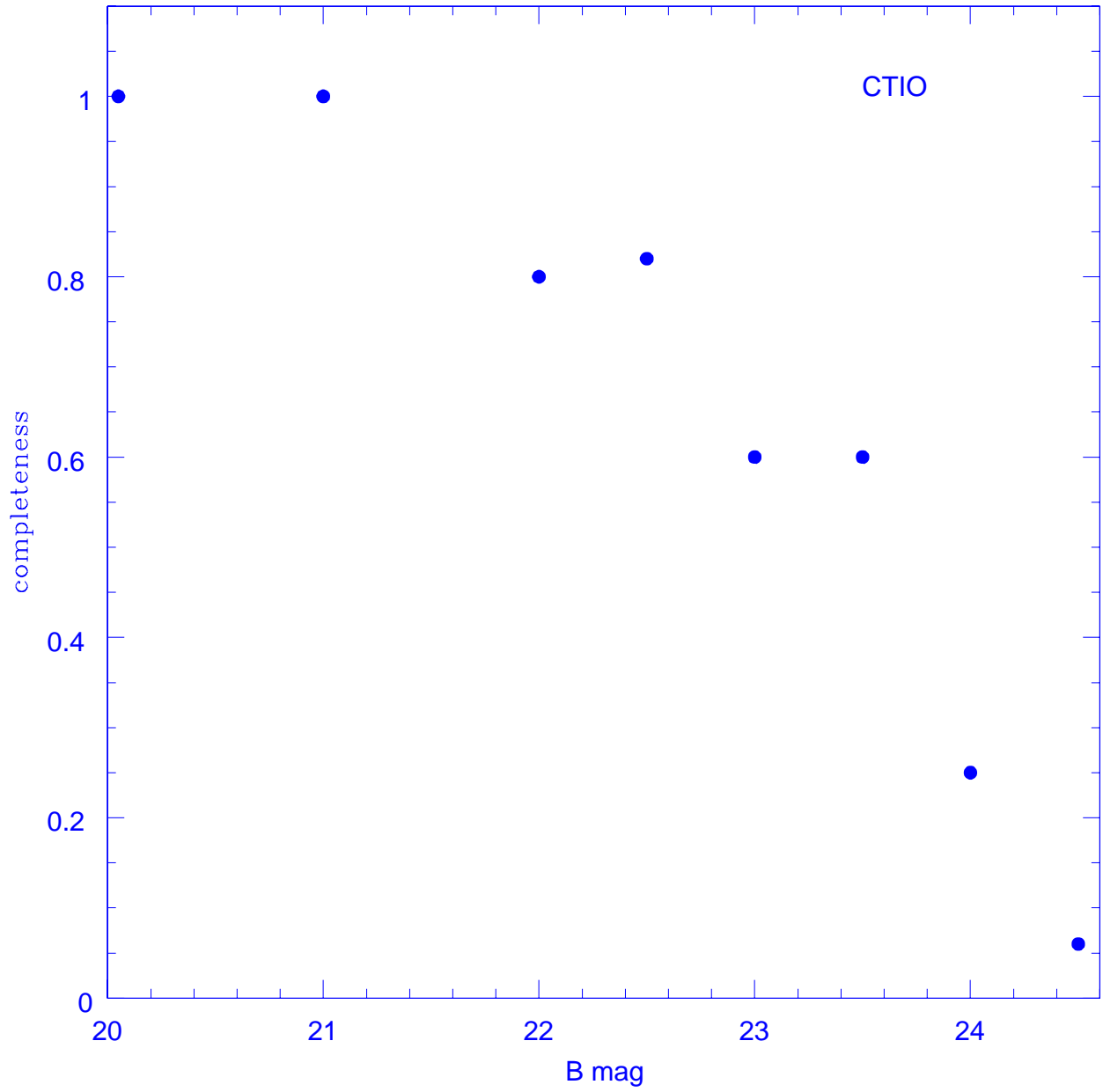


Fig. 7.—

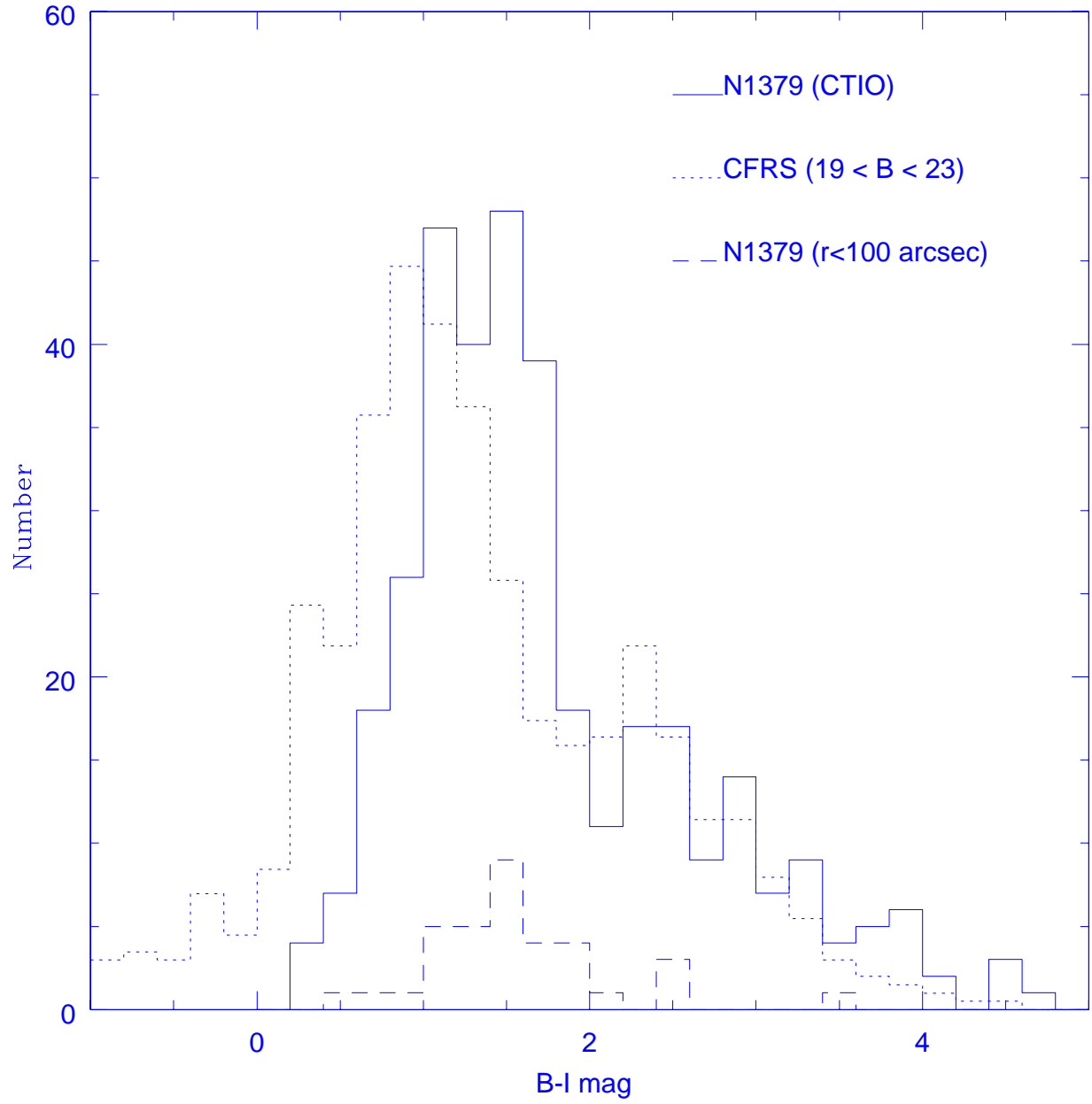


Fig. 8.—

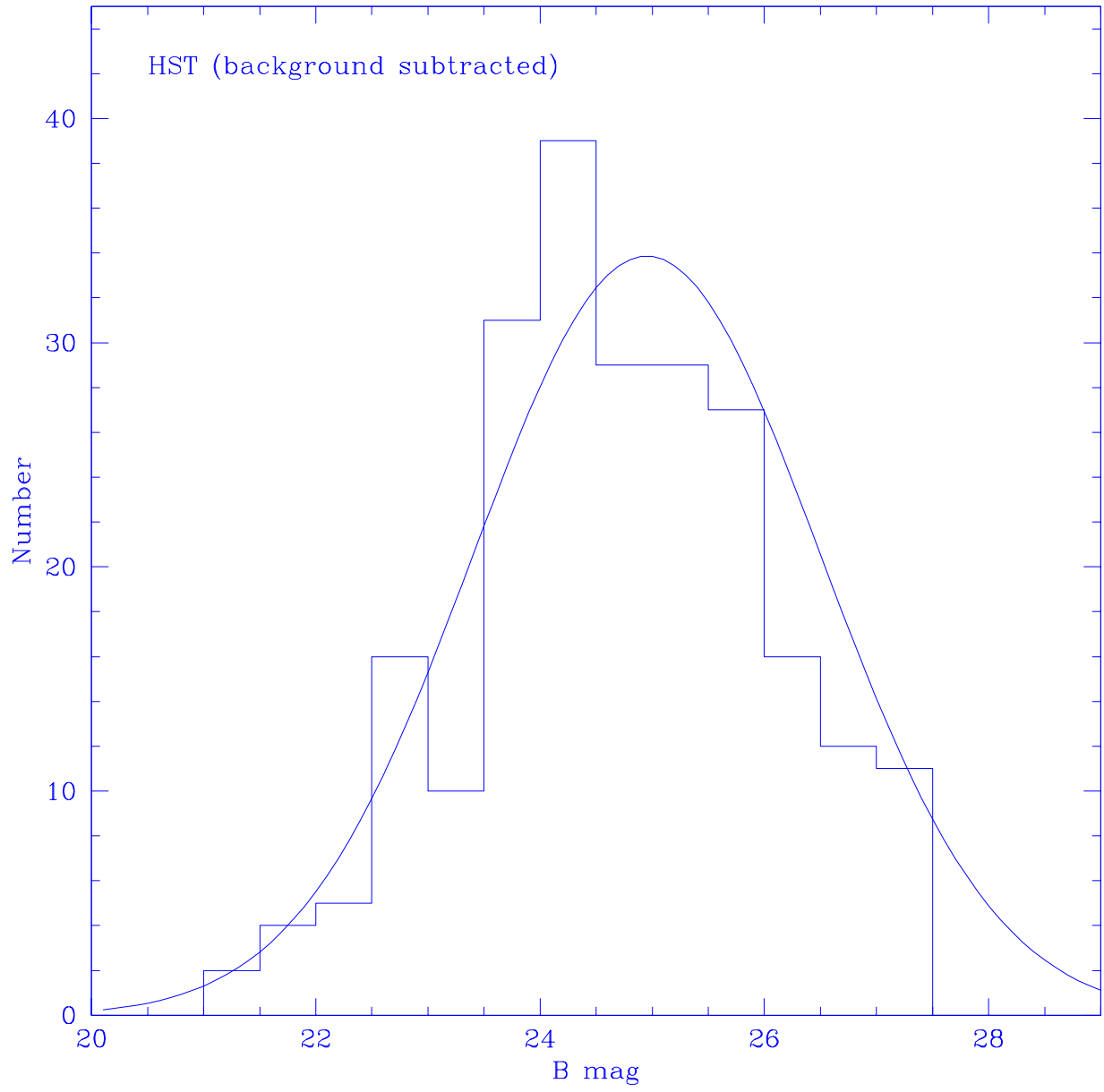


Fig. 9.—

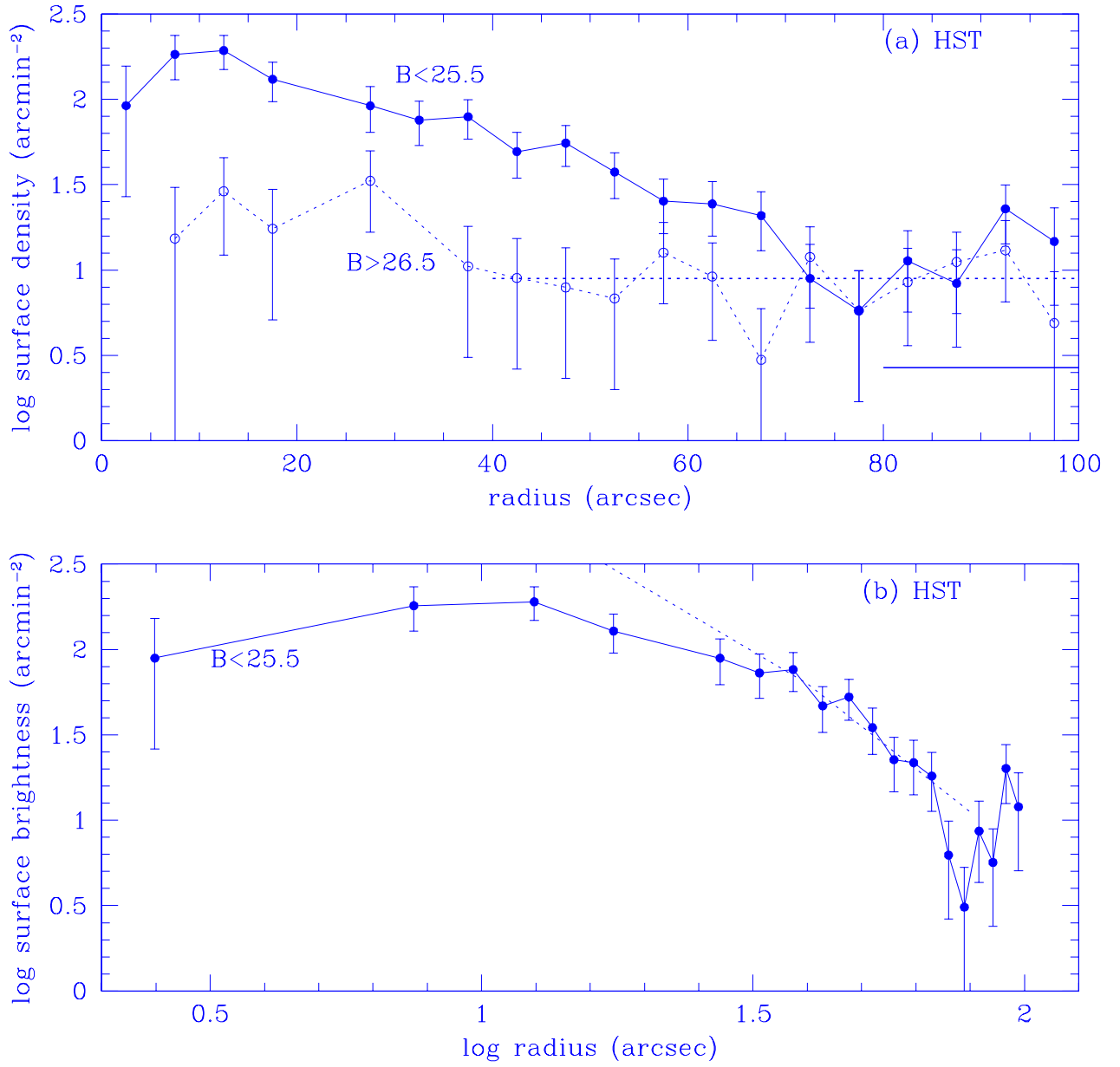


Fig. 10.—

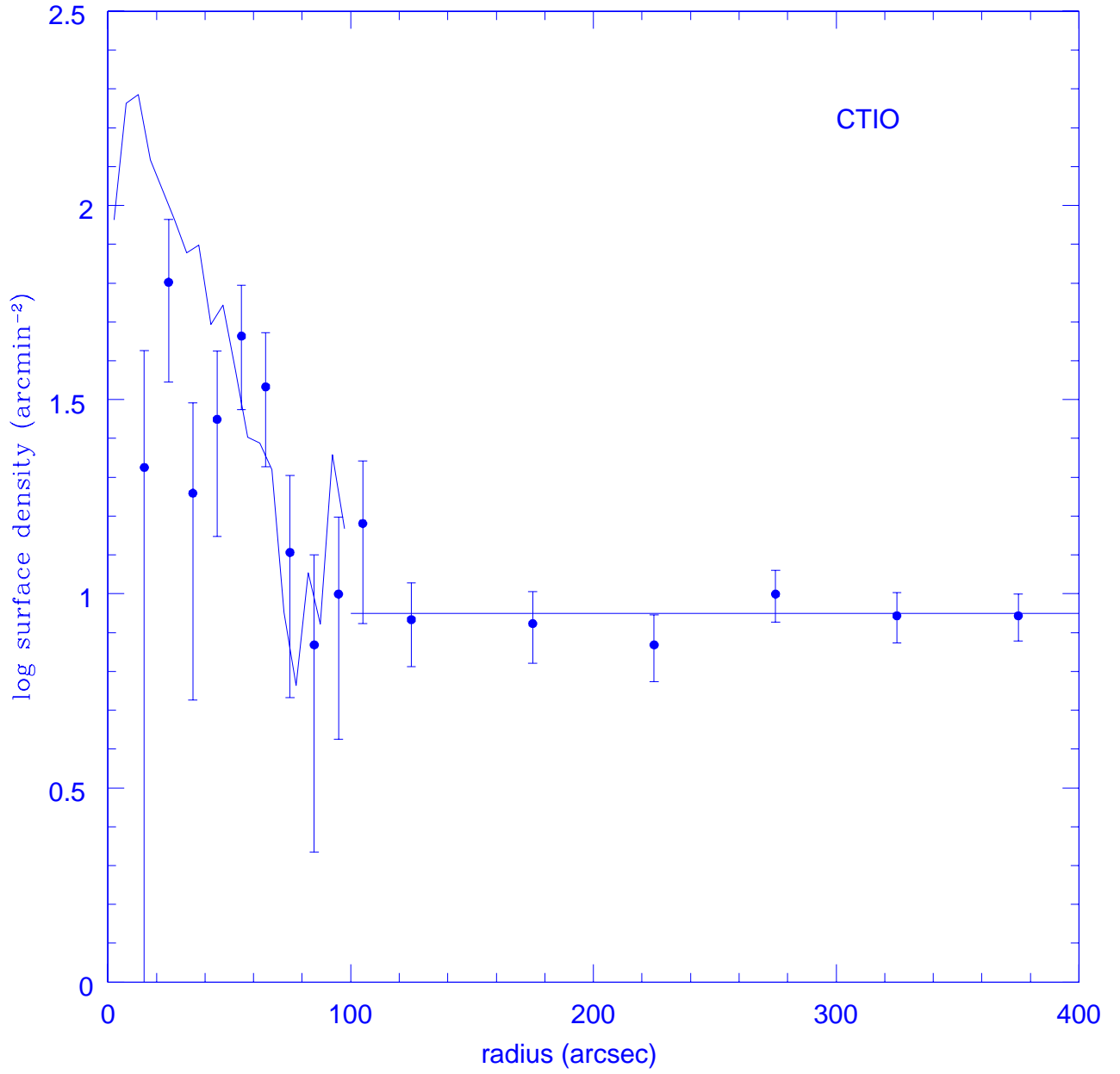


Fig. 11.—

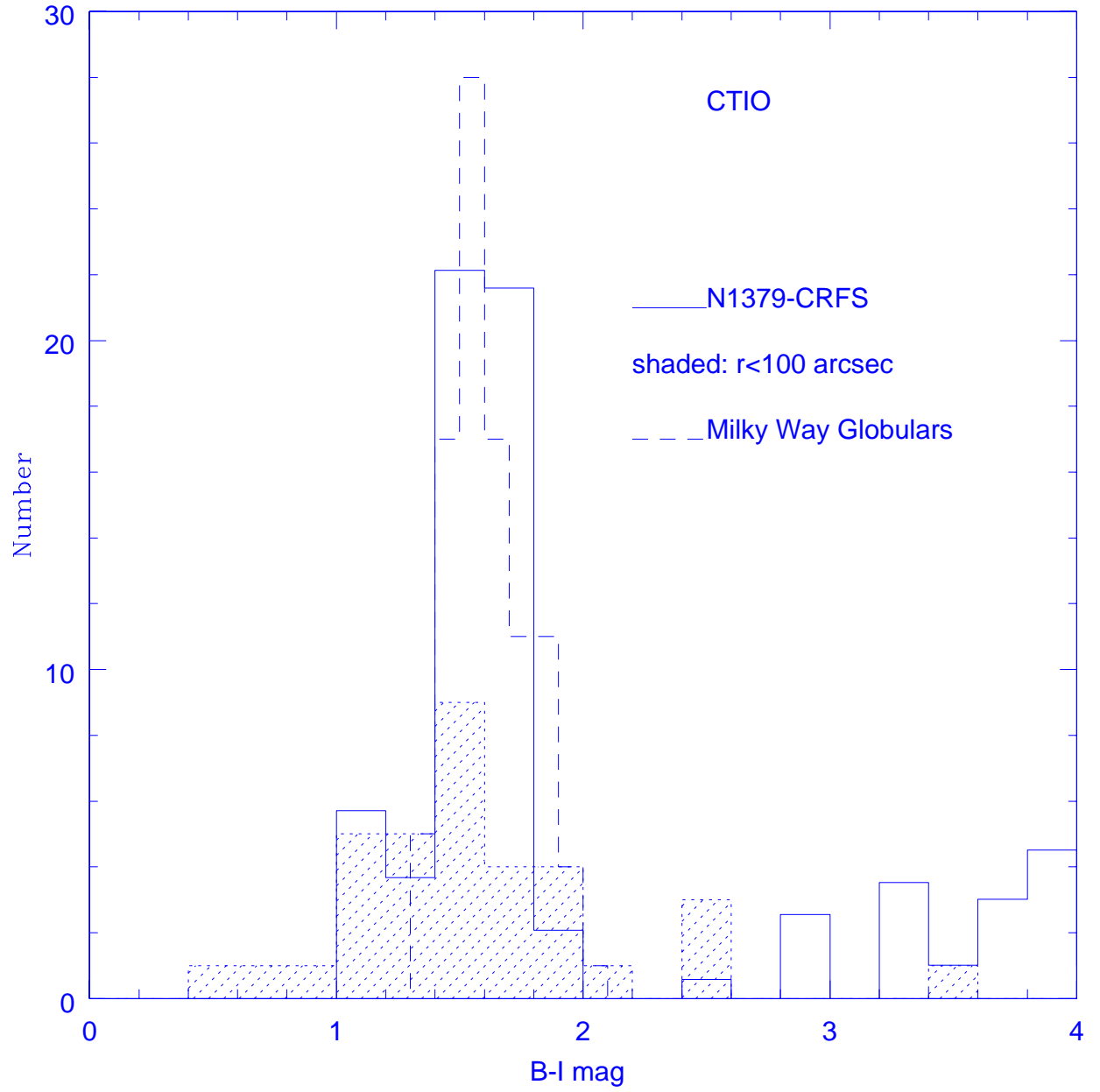


Fig. 12.—